



# Effect of cutting parameters and tool rake angle on the chip formation and adiabatic shear characteristics in machining Ti-6Al-4V titanium alloy

Anhai Li<sup>1,2</sup> · Jian Zang<sup>1</sup> · Jun Zhao<sup>1,2</sup>

Received: 31 August 2019 / Accepted: 2 March 2020 / Published online: 7 April 2020  
© Springer-Verlag London Ltd., part of Springer Nature 2020

## Abstract

Ti-6Al-4V titanium alloy is widely used in aeronautical parts and the high-efficiency machining and manufacturing process is surely a challenging work. The cutting parameters' proper selection and tool geometric angles' adoption will affect the material removal process in terms of chip formation and machined surface formation processes. In this paper, Abaqus finite element software was utilized to model and simulate the Ti-6Al-4V titanium alloy cutting process. The setting and selection of the constitutive model, material failure criterion, friction attribute, and heat transfer model make sure that the simulation is more in line with the actual cutting process. The correctness of the simulation model is verified by comparing the cutting forces and chip morphological characteristics obtained by the simulation with the experiments. Then, the effect of cutting parameters and tool rake angle on the chip formation and analyses of the adiabatic shear banding process was investigated, by using the machining simulation tests with different tool rake angles and cutting speeds. Results illustrate that the chip segmentation degree increases with the increase of cutting speed and feed rate, while it decreases with the increase in rake angle. The adiabatic shear-banding chip formation mechanisms were revealed by analyzing the relationship between shear strain, shear stress, chip segmentation degree, and high-temperature shear zone in undeformed plot contours. The serrated chip formation process when machining titanium alloy accompanies with the dramatic changes of shear strain and stress in adiabatic shear banding.

**Keywords** Ti-6Al-4V titanium alloy · Adiabatic shear · High-temperature zone · Rake angle

## 1 Introduction

Adiabatic shear is a special phenomenon that the sharp deformation takes place in a short period. Adiabatic shear is the cause of serrated chip formation [1]. Due to the continuous formation of the adiabatic shear bands, the cutting system vibrates and cutting force fluctuates during the cutting process; these unstable factors will have an impact on the cutting process. The cutting force, cutting temperature, tool life, machining-induced surface

integrity, and other aspects of high-speed cutting process will be affected by the formation of serrated chips, so it is necessary to make a clear understanding of adiabatic shear.

During the formation of adiabatic shear band, the material endures high-speed load and the local zone occurs severe deformation, the heat generated from deformation softening material to promote further deformation [2]. Zener and Hollomon first put forward the causes of the formation of adiabatic shear bands in 1946 [3], which are considered the result of competition between hardening and thermal softening during material deformation. Recht [4] interpreted it as adiabatic shear and used the critical strain rate as a necessary condition for the shear failure of titanium alloy; the essence is that the adiabatic temperature rise in the plastic deformation zone at high strain rate, and the degree of material softening is greater than the degree of strain hardening. Similar to crack propagation, the formation of adiabatic shear bands also includes initiation, expansion, and fracture process [5–7]. The mechanism of deformation of adiabatic shear has always been the focus of the metal cutting process.

✉ Jun Zhao  
zhaojun@sdu.edu.cn

<sup>1</sup> Key Laboratory of High Efficiency and Clean Mechanical Manufacture of MOE, School of Mechanical Engineering, Shandong University, Jinan 250061, People's Republic of China

<sup>2</sup> National Demonstration Center for Experimental Mechanical Engineering Education (Shandong University), Jinan 250061, People's Republic of China

**Fig. 1** The finite element cutting simulation model

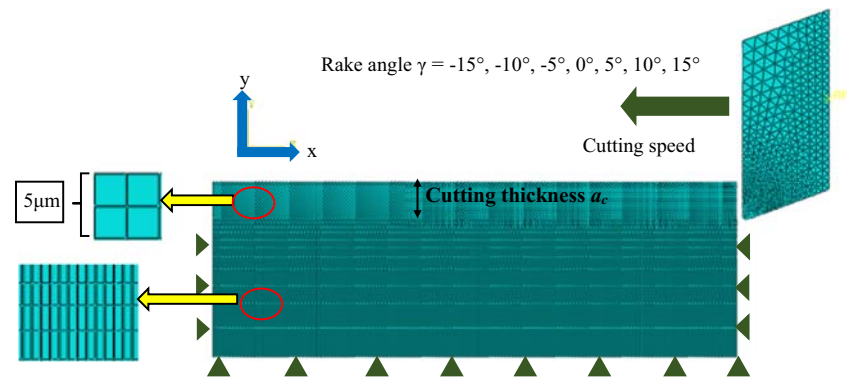
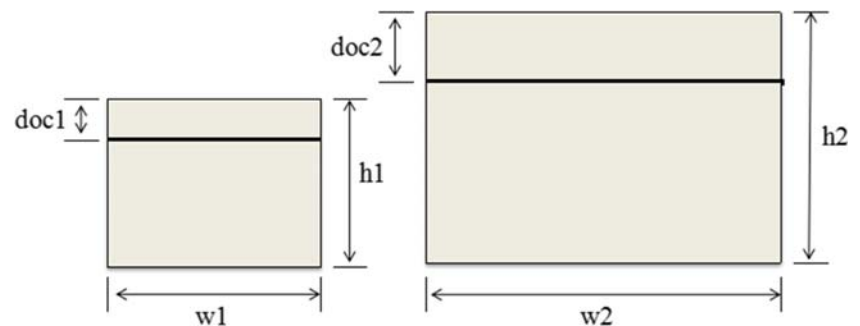


**Fig. 2** The workpiece dimensions with different mesh feature sizes  $L_1$  and  $L_2$



In 1964, Recht [4] argued that the initiation of adiabatic shear instability was attributed to the fact that the strain rate exceeded a critical value and established a critical strain rate criterion. Culver [8] established a critical strain on adiabatic shear in 1973. Batra and Kim [9] put forward the critical stress criterion in 1992. Then, the thermo-plastic properties and adiabatic shear deformation of Ti-6Al-4V were studied based on the critical stress criterion [10]. The strain and strain rate bivariate criterion was proposed. The shear strain of the serrated chip was theoretically analyzed by Hoffmeister [11] and carried out by the cutting experiment; it was found that the speed reaches a certain value, the serrated chip in the adiabatic shear zone fracture. Turly [12] holds that the strain of serrated chips is mainly composed of unit shear strain and adiabatic shear strain, and the value of the two strains is characterized by the morphological parameters of the chip. Miguélez [13] used the finite element model to analyze the adiabatic shear band of Ti-6Al-4V and obtained the strain distribution of the serrated chip. The adiabatic shear band in the energy model is built and investigated through chip morphology examination and high-speed

machining tests [14] and found that due to the occurrence of adiabatic shear, the serrated chip is formed, while the isolated segment is formed due to adiabatic shear fracture.

The chip formation process and adiabatic shear characteristics of titanium alloy Ti-6Al-4V are a research hotspots in titanium alloy machining process, because the chip generation process is affected by material flowing and fracture mechanisms [15], microstructural evolution behavior [16, 17], cutting parameters [18], tool wear, and tool geometric angles [19, 20]. The scientific understanding of the chip formation process is the premise of investigating the machining induced surface integrity, and exploring the in-depth mechanisms to the material separation and chip formation will advance the effectiveness of controlling the machining surface quality [21, 22]. The thermal conductivity of the workpiece material will increase with the temperature rising; this will affect the cutting temperature rise, the heat diffusion rate, the tool-chip contact surface, and the chip morphology [23]. To obtain different chip shapes, Li and Xu [24] conducted cutting experiments of Ti-6Al-4V titanium alloy, and the energy barrier formed adiabatic shear band was calculated. It is concluded that the adiabatic shear sensitivity and chip morphology can be predicted by calculating the energy barrier to provide the basis for the selection and the design of the materials with different adiabatic shear sensitivity. The critical criterion of adiabatic shear and the shape of serrated chips are studied in the studies mentioned above, but the mechanism of chip formation and the stress and strain characteristics under different cutting conditions are not considered.

**Table 1** Constitutive model parameters of Ti-6Al-4V titanium alloy [28]

$A$ (MPa)	$B$ (MPa)	$n$	$C$	$m$
782	498	0.28	0.028	1

**Table 2** Physical properties of Ti-6Al-4V titanium alloy [29]

Density (kg/m <sup>3</sup> )	Elastic modulus (GPa)	Poisson’s ratio	Thermal conductivity (W/m K)	Specific heat (J/kg K)
4430	109 (50 °C)	0.34	6.8 (20 °C)	611 (20 °C)
	91 (250 °C)		7.4 (100 °C)	624 (100 °C)
	75 (750 °C)		9.8 (300 °C)	674 (300 °C)
			11.8 (500 °C)	703 (500 °C)

So in this paper, the finite element software Abaqus is used to establish the simulation model, and the serrated chip formation in different tool rake angles and different cutting speeds are studied. It provides some theoretical guidance for the cutting of Ti-6Al-4V. Besides, the stress and strain characteristics in adiabatic shear bands are investigated. Through the cutting simulation, the stress and strain of the shear zone are studied with the change of the rake angle of the cutting tool, and the influence of the rake angle on adiabatic shear is further explained. It is mainly focused on the formation mechanism of the serrated chip, providing the basis for the selection of cutting edge and cutting speed in the actual machining process by using the finite element model. This provides a theoretical basis for titanium alloy processing and manufacturing enterprises, so as to better control the formation of serrated chip and improve the processing quality by applying reasonable cutting parameters and appropriate cutting tool rake angle. The new data and analysis results produced will be of value to practicing engineers in the aeronautical industry and help comprehensively advance the scientific understanding of adiabatic shear and serrated chip formation during high-speed machining titanium alloy.

## 2 Finite element machining simulation model and experimental validation

### 2.1 Finite element machining simulation model

#### 2.1.1 Establishment of cutting model

The two-dimensional cutting model can simplify the cutting process and easy to analyze. In order to adapt the thermo-mechanical coupling in the cutting process, the workpiece grid uses the planar quadrilateral continuum elements (CPE4RT) [14, 25]. In the cutting process, grid cell removal technology was used to meet the chip and workpiece separation. In order to eliminate the deformation and wear of the tool material, the tool is set as a rigid body during the modeling process, so that the workpiece

**Table 3** Johnson-Cook failure parameters of Ti-6Al-4V titanium alloy [31]

$D_1$	$D_2$	$D_3$	$D_4$	$D_5$
-0.09	0.25	-0.5	0.014	3.87

material can be analyzed more accurately. Figure 1 shows the established finite element cutting model; the horizontal direction of the bottom edge of the workpiece is constrained separately from the vertical direction and the horizontal direction. Select the reference point on the right side of the cutting tool and apply the cutting speed to the reference point. In order to improve the efficiency of cutting simulation, the mesh size of the undeformed layer to be cut is  $5\ \mu\text{m} \times 5\ \mu\text{m}$ , and the matrix part of the material model is set as a gradient dimensional mesh. Moreover, in order to evaluate the influence of tool rake angle on the machining process, seven kinds of cutting tools with rake angles  $\gamma = -15^\circ, -10^\circ, -5^\circ, 0^\circ, 5^\circ, 10^\circ,$  and  $15^\circ$  are adopted in the simulation process. The external boundary temperature is set to  $20\ ^\circ\text{C}$ , cutting thickness  $a_c = 0.1\ \text{mm}$ , tool flank angle  $= 7^\circ$ , and the tool edge radius  $25\ \mu\text{m}$ .

It is worth mentioning that the meshing process of the machining model is ensured by the energy density method. The dimension of the meshing element is an essential parameter to control the accuracy of the simulation results. In order to reduce or eliminate the influence of element mesh size on the simulated result, the material stress-strain relationship should possess the same failure energy density under different simulation conditions. For different feed conditions, Fig. 2 shows the workpiece dimensions for a two-dimensional cutting simulation model with the different mesh feature sizes  $L_1$  and  $L_2$  (where  $doc$  is the depth of cut,  $h$  and  $w$  are the height and the width of the workpiece). It is necessary to maintain the same mesh distribution of the workpiece in the actual

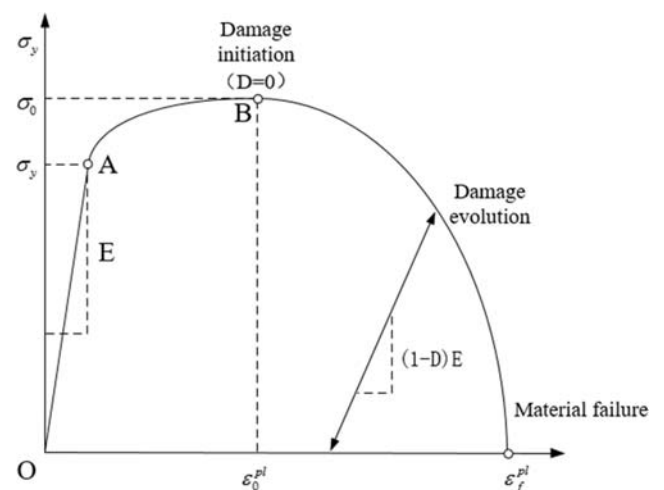


**Fig. 3** The stress-strain curve under different high strain rates

**Fig. 4** Orthogonal cutting experimental setups



simulation process. The mesh number of each part remains unchanged, and the toughness failure can be adjusted according to the mesh size of the element to make it meet the following relationship.

And even if the cutting conditions are different or the thickness of the cutting layer is different, the method of making the number of meshes in the chip layer the same can also ensure that there are enough nodes to calculate the physical variables in the

**Fig. 5** The simulated result in the chip formation process,  $v = 100 \text{ m/min}$ ,  $f = 0.1 \text{ mm/rev}$ . Mises stress (a), cutting temperature (b), equivalent plastic strain (c), and main cutting force (d)

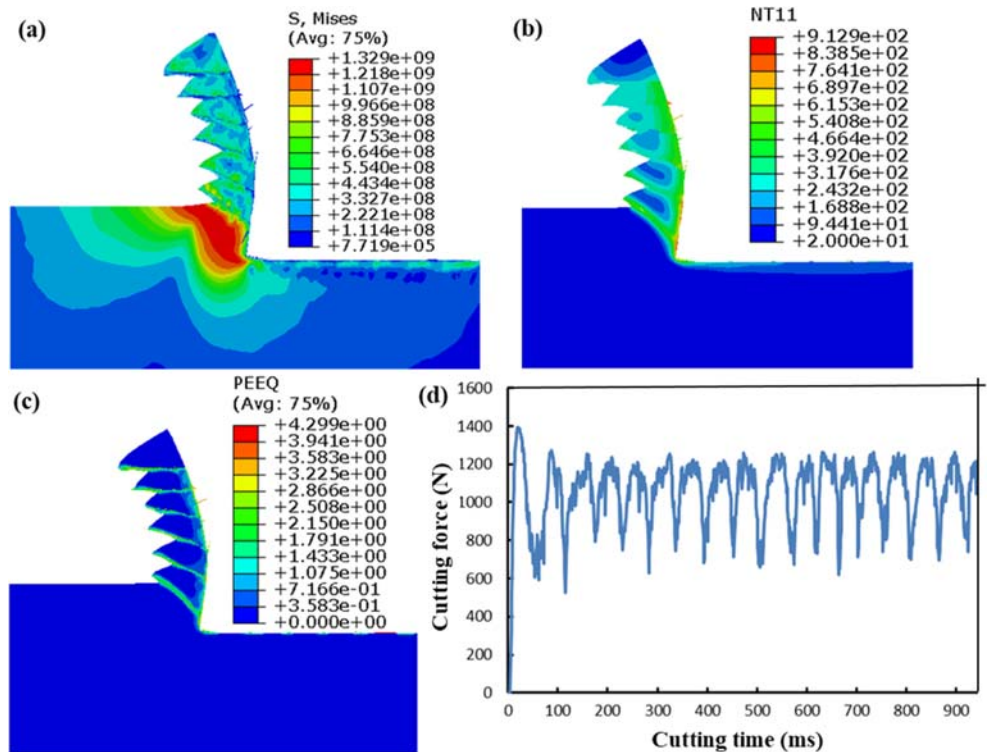
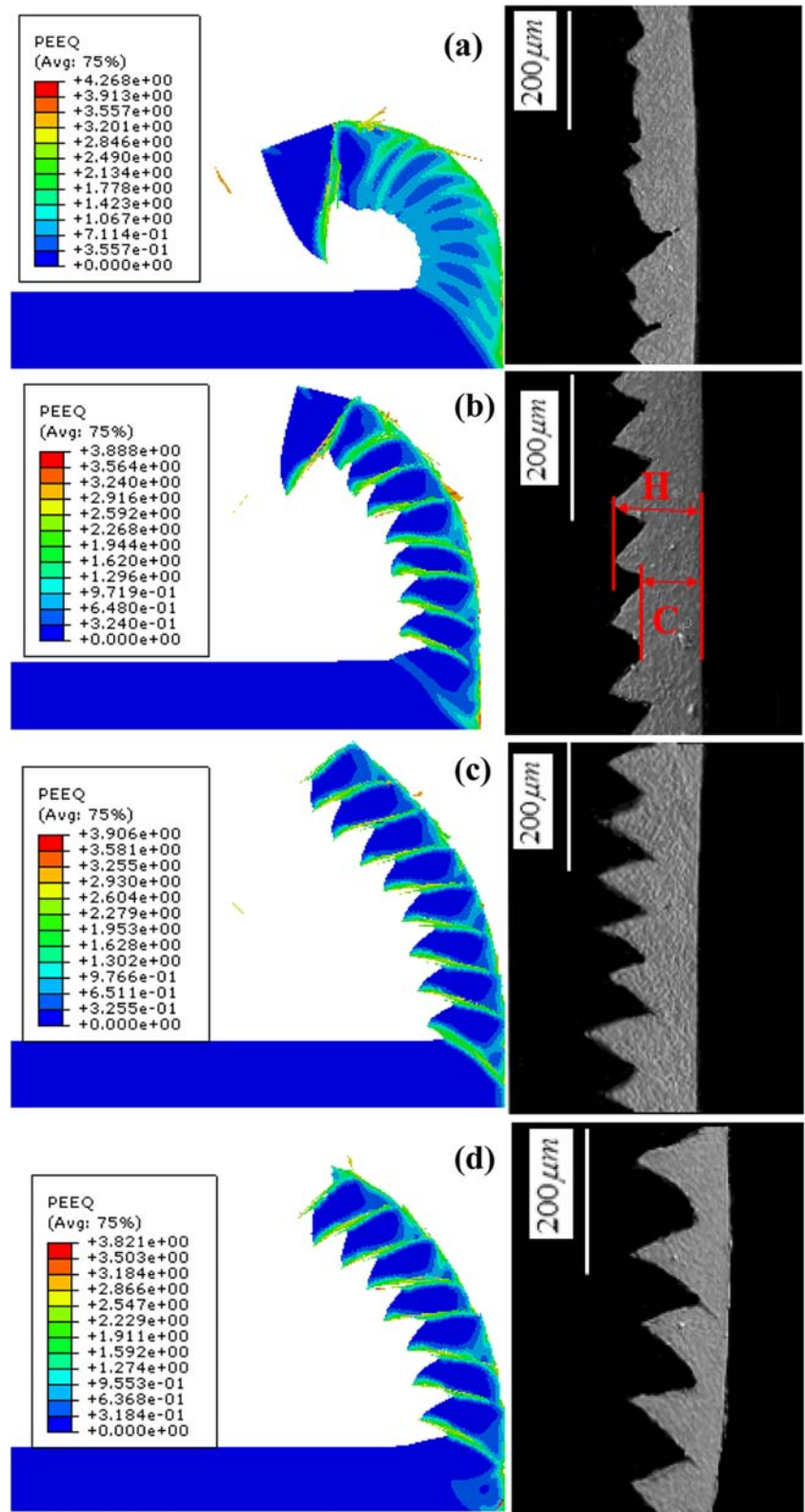




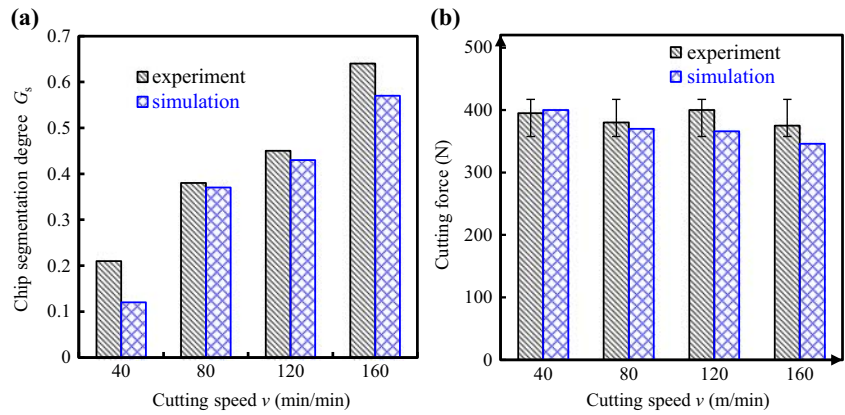
**Fig. 6** The chip morphology obtained from simulation and experiment.  $v = 40$  m/min (a);  $v = 80$  m/min (b);  $v = 120$  m/min (c);  $v = 160$  m/min (d)



chip, improve the calculation accuracy, and ensure the accuracy of the simulation results. So by using the energy density method, the meshing distribution of the workpiece can be set to be the

same. At the same time, the toughness failure energy can be adjusted according to the mesh size to eliminate the influence of mesh feature size on the simulation results.

**Fig. 7** Variation of simulation results compared with experiments under different cutting speeds ( $f=0.1$  mm/rev). Segmentation degree (a). Cutting force (b)



**2.1.2 Material constitutive model and material failure criterion**

The constitutive relationship is the basis for studying the dynamic mechanical behavior of materials. In the cutting process, the material usually occurs high strain, high strain rate deformation process, and accompanied by high-temperature environment. In many constitutive relations, the Johnson-Cook constitutive model is commonly used in finite element modeling, mainly due to its simultaneous consideration of strain, strain rate, and temperature on the flow stress, especially suitable for high strain rate conditions  $10^2\sim 10^6$  [26]. In this paper, the Johnson-Cook constitutive model is adopted; the expression is as follows [27]:

$$\sigma = (A + B\varepsilon^n) \left( 1 + C \ln \frac{\dot{\varepsilon}}{\dot{\varepsilon}_0} \right) \left[ 1 - \left( \frac{T - T_r}{T_m - T_r} \right)^m \right] \quad (1)$$

where  $\sigma$  is the flow stress,  $\varepsilon$  is the equivalent plastic strain,  $\dot{\varepsilon} / \dot{\varepsilon}_0$  is the dimensionless plastic strain rate,  $\dot{\varepsilon}_0$  is the reference strain rate,  $n$  is the strain hardening rate index,  $A$  is the initial yield stress,  $B$  is the hardening coefficient,  $C$  is the strain rate sensitivity coefficient,  $m$  is the temperature softening index,  $T_r$  is the lowest experimental temperature, and  $T_m$  is the material melting temperature. The specific values of the parameters are shown in Tables 1 and 2.

Based on the equivalent plastic strain of the unit integral point, the failure parameters are defined by Johnson-Cook failure criteria [30], expressed as Eq. (2):

$$w = \sum \frac{\Delta \bar{\varepsilon}}{\bar{\varepsilon}_f} \quad (2)$$

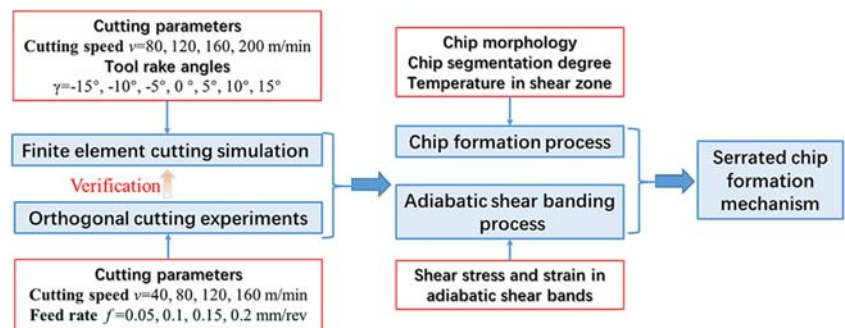
where  $\Delta \bar{\varepsilon}$  is the equivalent strain increment, and  $\bar{\varepsilon}_f$  is the equivalent strain, expressed as Eq. (3).

$$\bar{\varepsilon}_f = \left[ D_1 + D_2 \exp \left( D_3 \frac{P}{\bar{\sigma}} \right) \right] \left[ 1 + D_4 \ln \frac{\dot{\varepsilon}_f}{\dot{\varepsilon}_0} \right] \left[ 1 + D_5 \frac{T - T_r}{T_m - T_r} \right] \quad (3)$$

It can be seen from the above equation that the value of the failure strain is determined by the  $\bar{\varepsilon}$ ,  $T$ , and the dimensionless stress ratio  $P/\bar{\sigma}$ , where  $P$  is the average of the three principal stresses and  $\bar{\sigma}$  is the equivalent stress.  $D_1, D_2, D_3, D_4$ , and  $D_5$  are the failure parameters, the specific values shown in Table 3. In the simulation process, the values of failure parameters are accumulated after each analysis step, when the failure parameter of the material  $w$  exceeds 1, the grid is judged to be invalid and disappears in the whole grid.

Figure 3 shows the stress-strain curve under different strain rates; it can be seen from the figure that the OA segment is the elastic deformation stage of the material, where  $E$  is the elastic modulus, and  $\sigma_y$  indicates the maximum stress in the material deformation stage. The curve AB is the stable plastic deformation stage of the material; at this time, the strain hardening effect of the material is greater than that of the heat softening.

**Fig. 8** Flowchart for analyzing chip formation and adiabatic shear banding processes



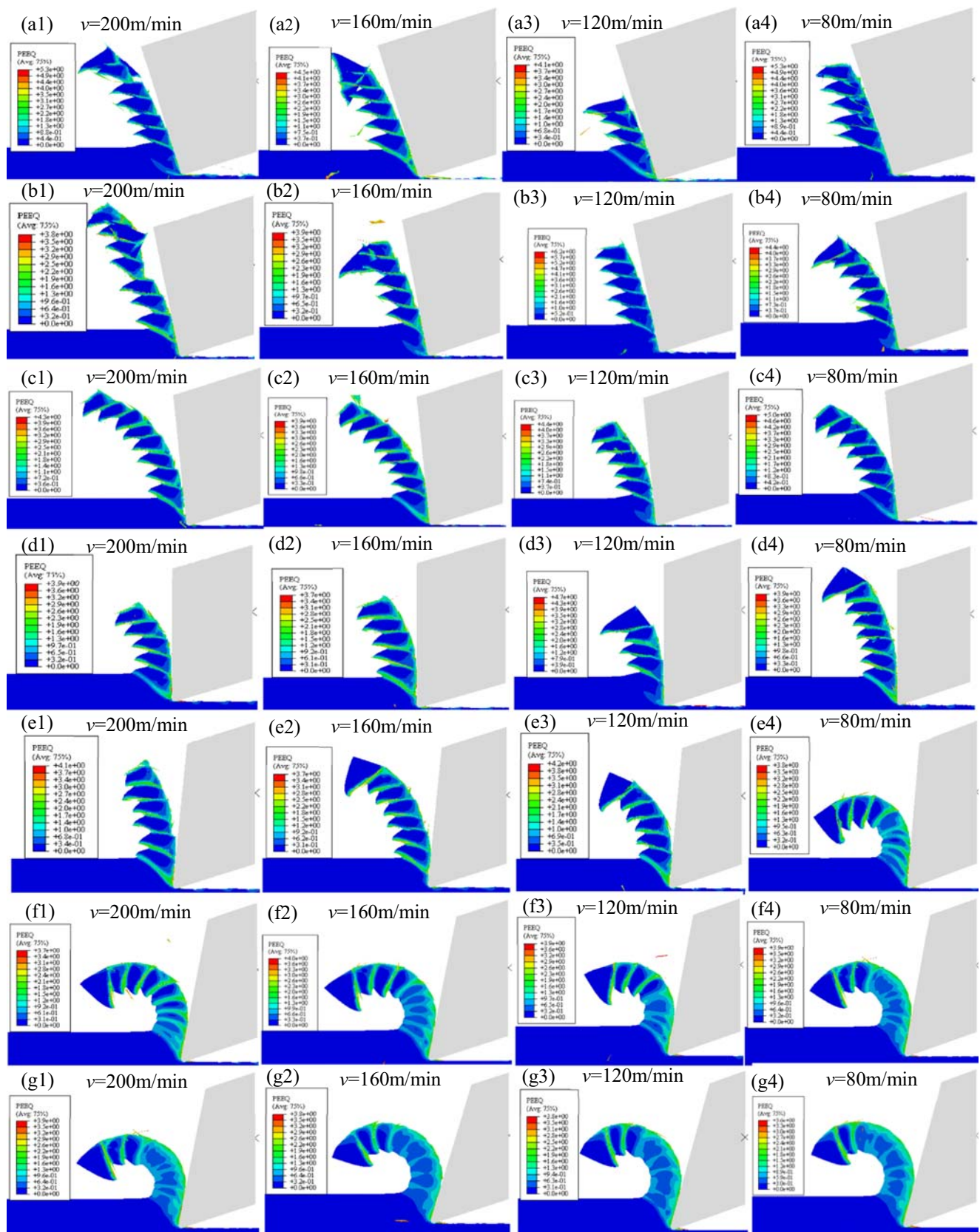


**Fig. 9** Chip morphologies of Ti-6Al-4V alloy in different rake angles and cutting speeds.  $\gamma = -15^\circ$  (a),  $\gamma = -10^\circ$  (b),  $\gamma = -5^\circ$  (c),  $\gamma = 0^\circ$  (d),  $\gamma = 5^\circ$  (e),  $\gamma = 10^\circ$  (f),  $\gamma = 15^\circ$  (g)



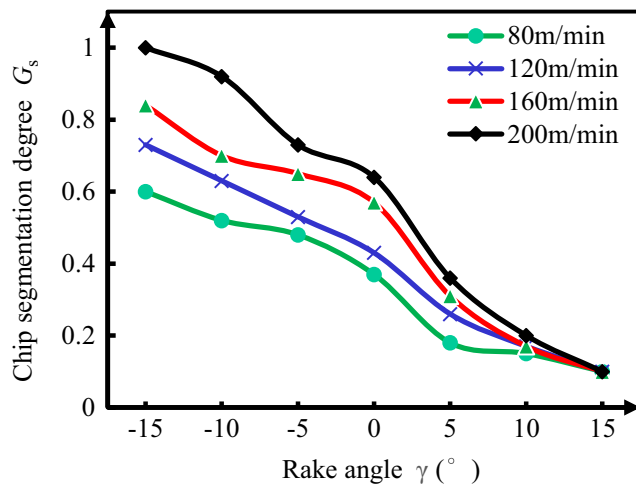


**Fig. 10** The variation of segmentation degree with different rake angle

The material starts to damage from point B, and the material fails with the increase of the strain.

### 2.1.3 Friction and heat transfer model

In the machining process, the friction between the material and tool has an important effect on the cutting force, the cutting temperature, and the residual stress of the machined surface. It is important to make a reasonable reflection of the friction in finite element software. During the cutting process, the friction is very complicated, which mainly includes the friction between the tool and the chip flow, the tool, and the machined surface.

In this paper, the modified Coulomb friction models are used to define contact friction. According to the contact state, the friction area is divided into two sections:

1. Adhesive area. The shear stress of the material  $\tau_f$  in this region is considered to be approximately equal to the shear yield strength of the material.
2. Slip area. The friction stress in this region is proportional to the normal stress, and the scale factor is the friction coefficient, which is set as  $\mu = 0.3$  [32].

$$\tau_f = \begin{cases} \tau_\gamma, \tau_\gamma \leq \mu\sigma_n \\ \mu\sigma_n, \tau_\gamma > \mu\sigma_n \end{cases} \quad (4)$$

## 2.2 Experimental validation of the simulation model

In order to verify the cutting model, the Ti-6Al-4V titanium alloy cutting experiment was carried out. Figure 4 shows the equipment of cutting tests, the cutting experiment was completed in the CKD6143H machining center, and Kistler 9257B dynamometer is used to test the cutting force in the orthogonal turning process. The cutting tool used is a top-notch tool holder (ISO grade NSR2525M3) equipped with a tough and ultra-fine-grain

tungsten-cemented carbide tool with an advanced PVD-AlTiN coating (grade KC5025 made by Kennametal Co. Ltd.). The cutting tool insert is a top-notch grooving and cut-off insert NG3156R, with a  $0^{\circ}$  tool rake angle, a  $7^{\circ}$  tool flank angle, a  $25\text{-}\mu\text{m}$  tool edge radius, and the tool cutting edge width is 3.96 mm. The workpiece in Fig. 4 is unprocessed and its dimensions are shown in the figure. During the machining, the workpiece bar diameter is  $\Phi 100$  mm; the cutting width is 2 mm; the grooving width is 3 mm; the radial feed is 0.1 mm/rev; and the cutting speeds are 40 m/min, 80 m/min, 120 m/min, and 160 m/min, respectively. The cutting condition is dry cutting. In order to eliminate the error of tool wear on the cutting results, the new sharp cutting tools are used in every cutting process. In order to acquire reliable test data, every cutting test was repeated at least three times to ensure the measured cutting force values are normal variation under different cutting conditions.

Figure 5 shows the stress, strain, and temperature fields obtained by finite element simulation of titanium alloy cutting at cutting speed  $v = 100$  m/min and feed  $f = 0.1$  mm/rev. From Fig. 5a, it can be seen that in the cutting process, the stress in the shear zone area is the largest and gradually decreases to both sides. Certain stresses remain on the machined surface. Figure 5b shows that the shear band of chips produces intense plastic deformation, and there is a slightly weaker plastic deformation on the machined surface. Figure 5c shows that chips take away most of the heat generated during cutting. These are consistent with the actual cutting process. Figure 5d is a diagram of the main cutting force in the simulation process under the conditions of cutting speed  $v = 100$  m/min and feed  $f = 0.1$  mm/rev.

The chips obtained from each orthogonal cutting experiment were collected and inserted to prepare the sample. After being polished and etched, the cross-sectional chip sample was observed under a scan electron microscope as shown in Fig. 6. Apparent serrated chips, especially at higher cutting speed range, can be seen obviously from the compared results of simulation and experiments, and the chip cross-sectional view under the same cutting speed condition exhibits similar geometric appearance.

In order to verify the correctness and accuracy of the simulation model, the segmentation degree  $G_s$  is used to quantitatively compare the experiment with the simulation.

$$G_s = \frac{H-C}{H} \quad (8)$$

where  $H$  represents the height of the chip crest, and  $C$  represents the height of the valley (Fig. 6b).

Figure 7 illustrates the variation of simulation results compared with experiments under different cutting speeds. Figure 7a shows the variation of segmentation degree  $G_s$  with different cutting speeds. Under the condition of different machining parameters, the trend of chip shape in the simulation and experiment is the same; when the cutting thickness is



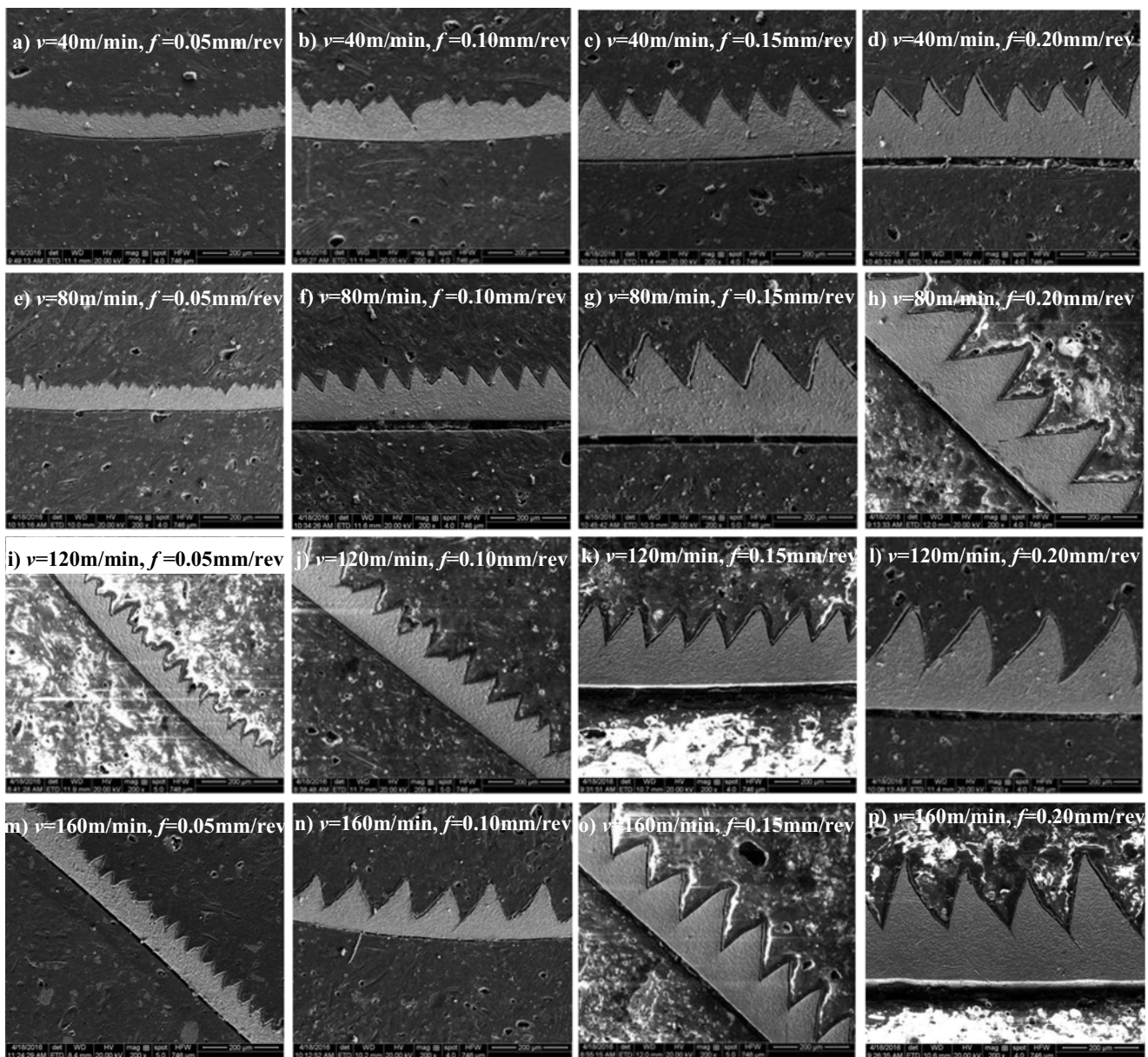


**Fig. 11** Chip cross-sectional morphological SEM images under different cutting parameters

0.1 mm and the cutting speed is 40 m/min, the chip shape obtained by simulation and experiment presents continuous strip chip, while with the speed of 80 m/min, 120 m/min, and 160 m/min, the chip shape changes from continuous strip chip to sawtooth chip, and the segmentation degree  $G_s$  increases with the increase of cutting speed. For the cutting force in the cutting simulation and the cutting force measured by the experiment shown in Fig. 7b, it can be seen that the cutting force measured by the experiment is slightly greater than the cutting force in the simulation when the cutting speed is 80 m/min, 120 m/min, and 160 m/min, and the cutting force in the experiment is smaller than the cutting force measured by simulation when the cutting speed is 40 m/min, and the relative error is smaller than the cutting force measured by simulation

due to the cutting tool wear in turning experiment and the measuring error of instrument and the machining system vibration. However, the error rates of the numerical results compared with the experimental test results were kept within 15%. Thus, it can be seen that the simulation is in good agreement with the experiment, and the simulation model is good and reliable to reproduce the chip formation process.

### 3 Chip formation and analyses of adiabatic shear banding process

Figure 8 indicates the flowchart for analyzing the chip formation and adiabatic shear banding processes. In order to acquire

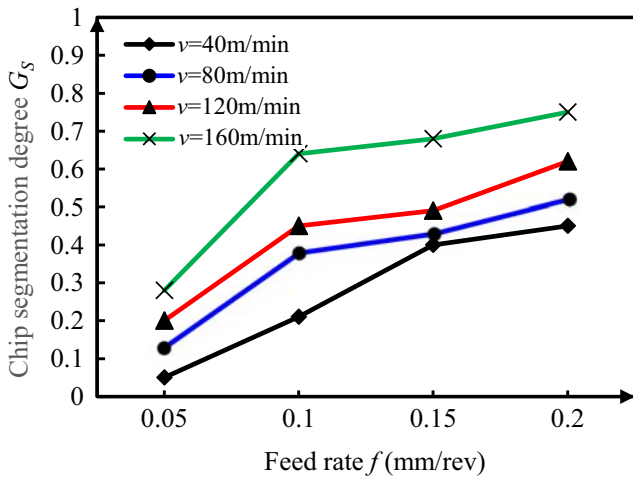


Fig. 12 Chip segmentation degree  $G_s$  under different cutting parameters

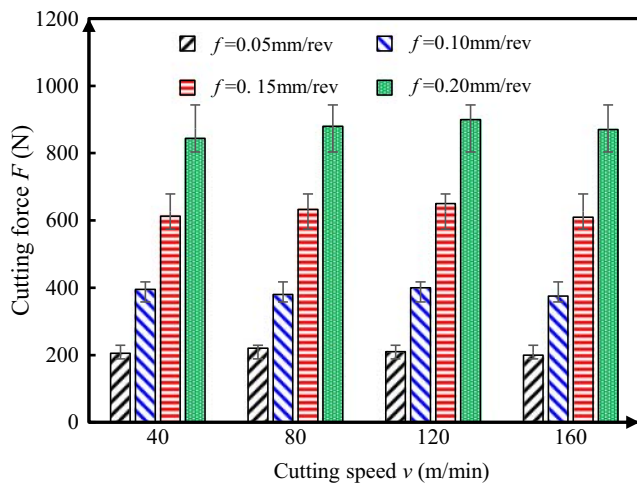


Fig. 13 Changes in cutting forces with different cutting speeds and feed rates

the results of chip formation and adiabatic shear banding process in machining Ti-6Al-4V titanium alloy, the finite element cutting simulation under different cutting parameters and tool rake angles was conducted, and the experiments under

different cutting speeds and feed rates were performed. And the chip morphology, chip segmentation degree, shear strain, shear stress, and temperature in the adiabatic shear zone were analyzed to reveal the serrated chip formation mechanisms in the formation and adiabatic shear banding processes.

### 3.1 Simulation results under different rake angles and cutting speeds

Figure 9 lists a pile of chip morphologies of Ti-6Al-4V alloy in different rake angles and cutting speeds. The rake angle is changed by the model, which is set to  $-15^\circ$ ,  $-10^\circ$ ,  $-5^\circ$ ,  $0^\circ$ ,  $5^\circ$ ,  $10^\circ$ , and  $15^\circ$ , respectively. The cutting speed is 80 m/min, 120 m/min, 160 m/min, and 200 m/min. As shown in Fig. 9, it can be seen that at a certain speed, the chips are gradually changed from serrated chips or unit chips to flow chips when the angle of the tool increases. With the increase in cutting speed, the segmentation degree of the chip is increasing. Figure 10 shows the variation of segmentation degree with the rake angle of the tool and the cutting speed. It can be seen that with the increase of the rake angle, the segmentation degree of the chip gradually reduced, and with the increase in cutting speed, the segmentation degree has a rising trend. In addition, when the rake angle of the cutting tool is  $0^\circ \sim 5^\circ$ , the segmentation degrees have the largest reduction.

### 3.2 Experimental results under different cutting parameters

The machined chips were collected and mounted to the cross-sectional view for measurement under a scanning electron microscope (SEM). Then, the chip cross-sectional morphological SEM images under different cutting parameters were comparably observed and listed in Fig. 11. Figure 12 shows the variation of sawtooth degree  $G_s$  with cutting speed and feed rate. It can be seen that the sawtooth degree of chips increases with the increase of cutting speed and feed rate.

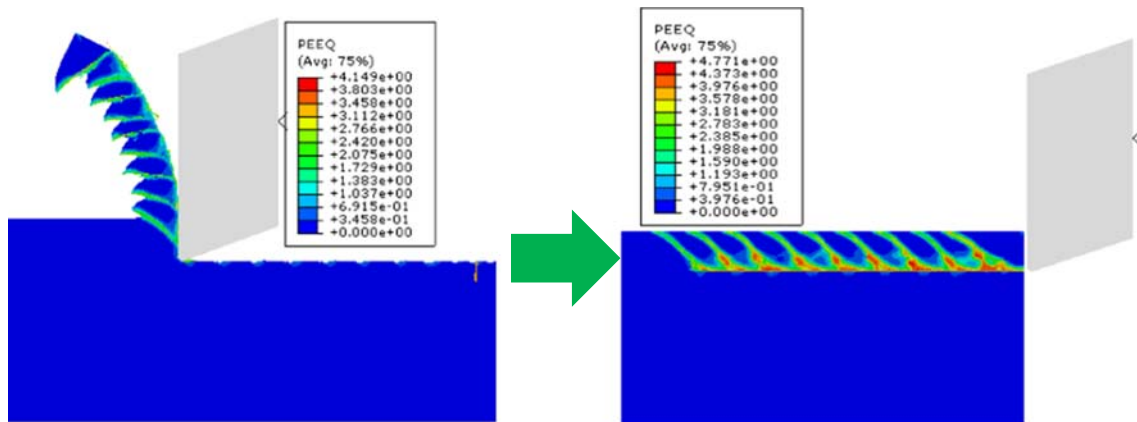


Fig. 14 Deformed shape transfer to undeformed shape

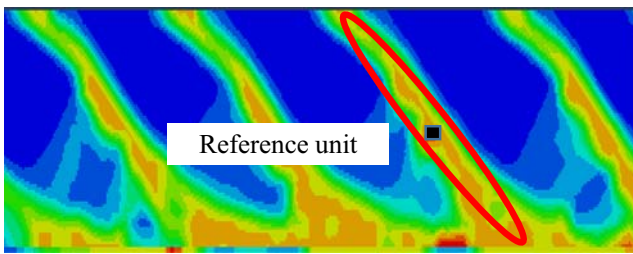


Fig. 15 The location of the reference unit in adiabatic shear bands

In the process of orthogonal turning, because the tangential force  $F_c$  in the direction of cutting speed is much larger than the feed force  $F_f$ , only the changing trend of the cutting force  $F_c$  with cutting speed and feed rate is discussed.

Figure 13 shows the cutting forces measured with different turning parameters. When the turning speed is 40 m/min, the cutting force increases from 205 to 844 N as the feed rate increases from 0.05 to 0.20 mm/rev. When the turning speed is the same, the cutting force increases with the increase of feed; when the feed rate is 0.05 mm/rev and the turning speed increases from 40 to 80 m/min, the cutting force increases from 205 to 220 N, and with the increase of turning speed to 160 m/min, the cutting force decreases to 200 N. With the increase of turning speed, the degree of material softening increases, which leads to the decrease in cutting force. When the feed rate increases, the chip thickness is relatively larger, and then the material removal rate and the friction in the contact area are increased; thus, the tool wear process is accelerated, and eventually the cutting force is significantly increased. But at the same time, the cutting temperature rise effect caused by a larger feed rate is relatively moderate compared with that caused by larger cutting speed [33]. So the feed rate is assumed to be constant, and it focused on the influence of cutting speed on the chip formation and adiabatic shear characteristics in the numerical investigation.

### 3.3 Characteristics of shear stress and strain in adiabatic shear bands

In order to explain the above results intuitively, the plot contours on an undeformed shape in the Abaqus are used to analyze the shear zone, as shown in Fig. 14; the physical state of each original position of the material can be observed clearly in undeformed shape, so that the adiabatic shear can be analyzed more accurately and clearly.

In the case of heat transfer continuously during the cutting process, the presence of the high-temperature zone is due to the material softening in the shear zone, resulting in uniform deformation under the action of the tool. Therefore, it is necessary to study the stress and strain of the material in the shear zone.

In the finite element model, it is complicated to analyze all the units in the shear zone. Therefore, with respect to the stress and strain in the simulation results, the intermediate unit in the

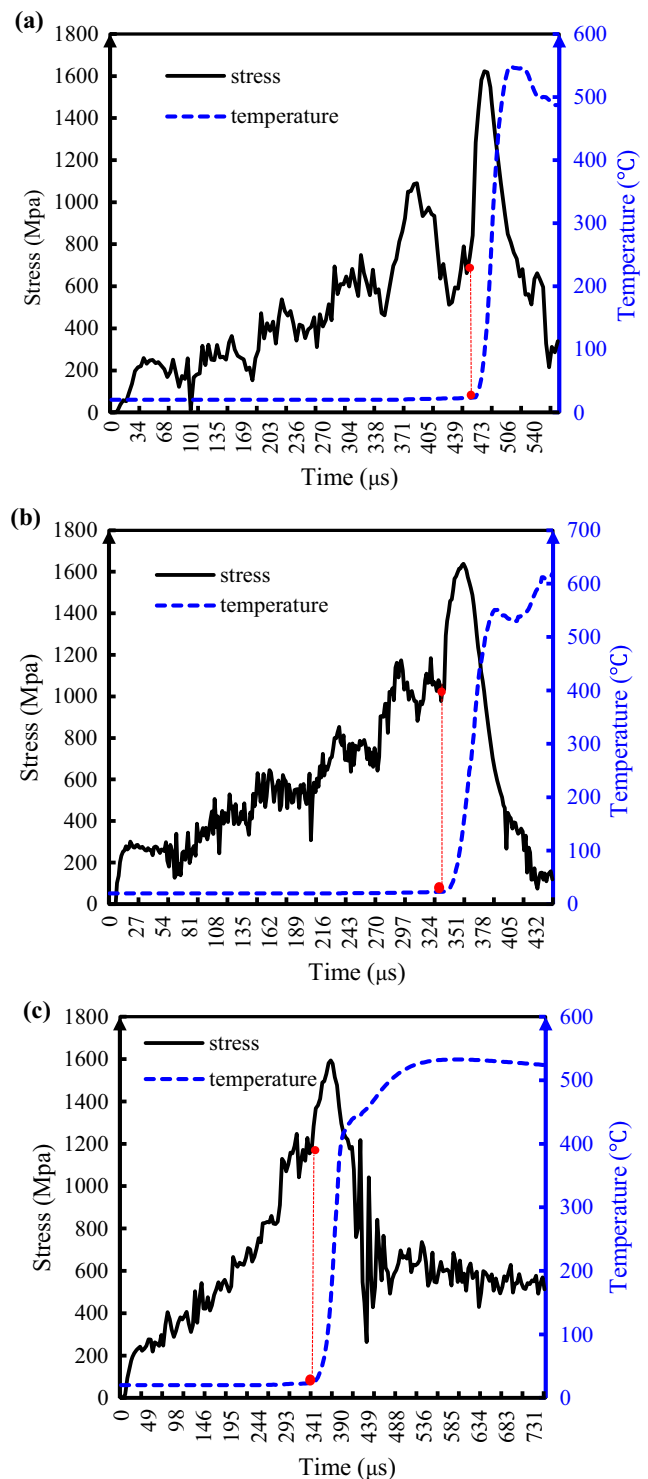
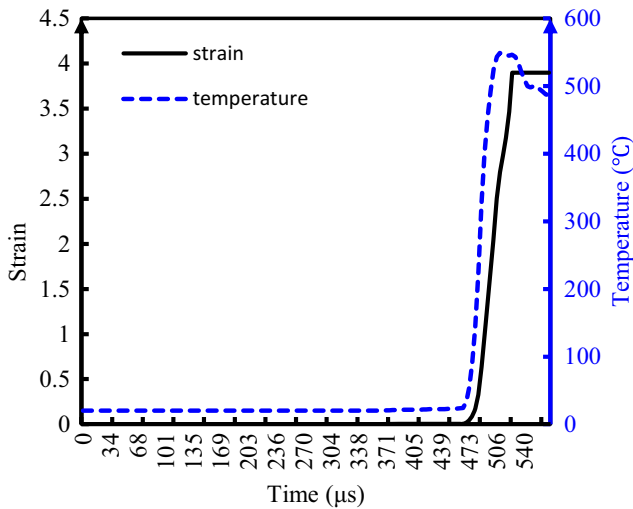


Fig. 16 Variation of stress and temperature in adiabatic shear bands,  $v = 100$  m/min,  $f = 0.1$  mm/rev.  $\gamma = -15^\circ$  (a),  $\gamma = 0^\circ$  (b),  $\gamma = 15^\circ$  (c)

shear zone is focused, as shown in the location of the reference unit in adiabatic shear bands in Fig. 15.

The stress, strain, and temperature of the reference unit in adiabatic shear bands, under the cutting parameters of  $v = 100$  m/min and  $f = 0.1$  mm/rev, can be seen from Fig. 16,





**Fig. 17** Variation of strain and temperature in adiabatic shear bands,  $\gamma = 0^\circ$ ,  $v = 100$  m/min,  $f = 0.1$  mm/rev

and the stress value of the reference unit increases at the beginning, reaches the maximum, and then decreases. The fluctuation range of the stress value are reduced when the rake angle of the tool increases. In addition, when the stress curve in the stage of the last ascension, the stress reference of the unit reaches the maximum value of about 1600 MPa, accompanied by the sharp temperature rise. In the cutting process, the persistent force acts on the workpiece with the movement of the cutting tool. Due to the deformation of the workpiece, the reference unit is also subject to a certain degree of stress, and the stress value is increasing with the tool close to the reference unit. Before the tool reaches the reference point, due to the adiabatic shear that occurred in the material, the reference unit of the stress value occurs a certain fluctuation, and the fluctuation of stress has a positive relationship with the degree of adiabatic shear.

**Fig. 18** Temperature distribution nephogram in the shear zone at different cutting speeds

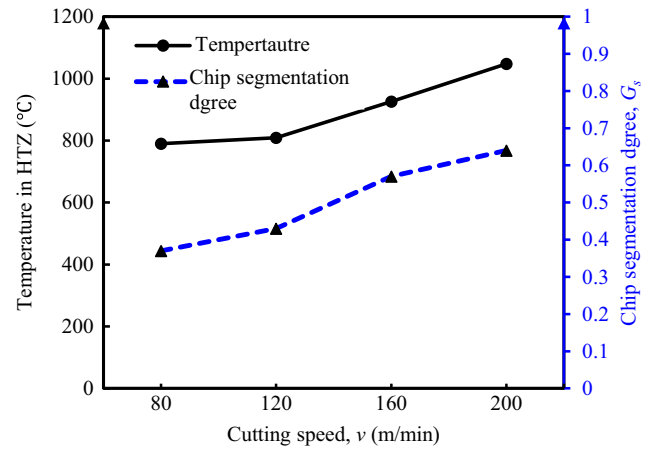
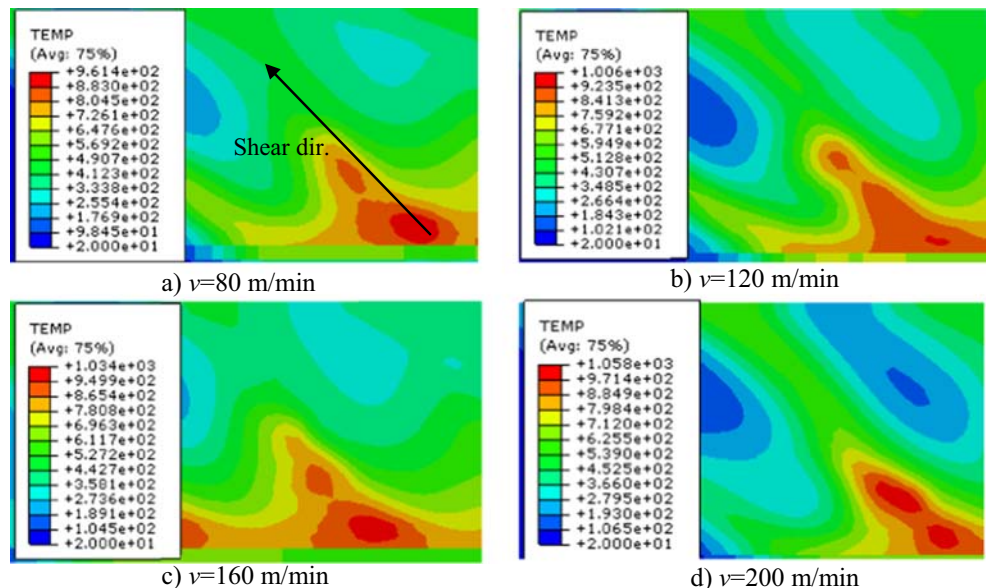


**Fig. 19** Temperature in HTZ and sawtooth degree of chips versus cutting speed

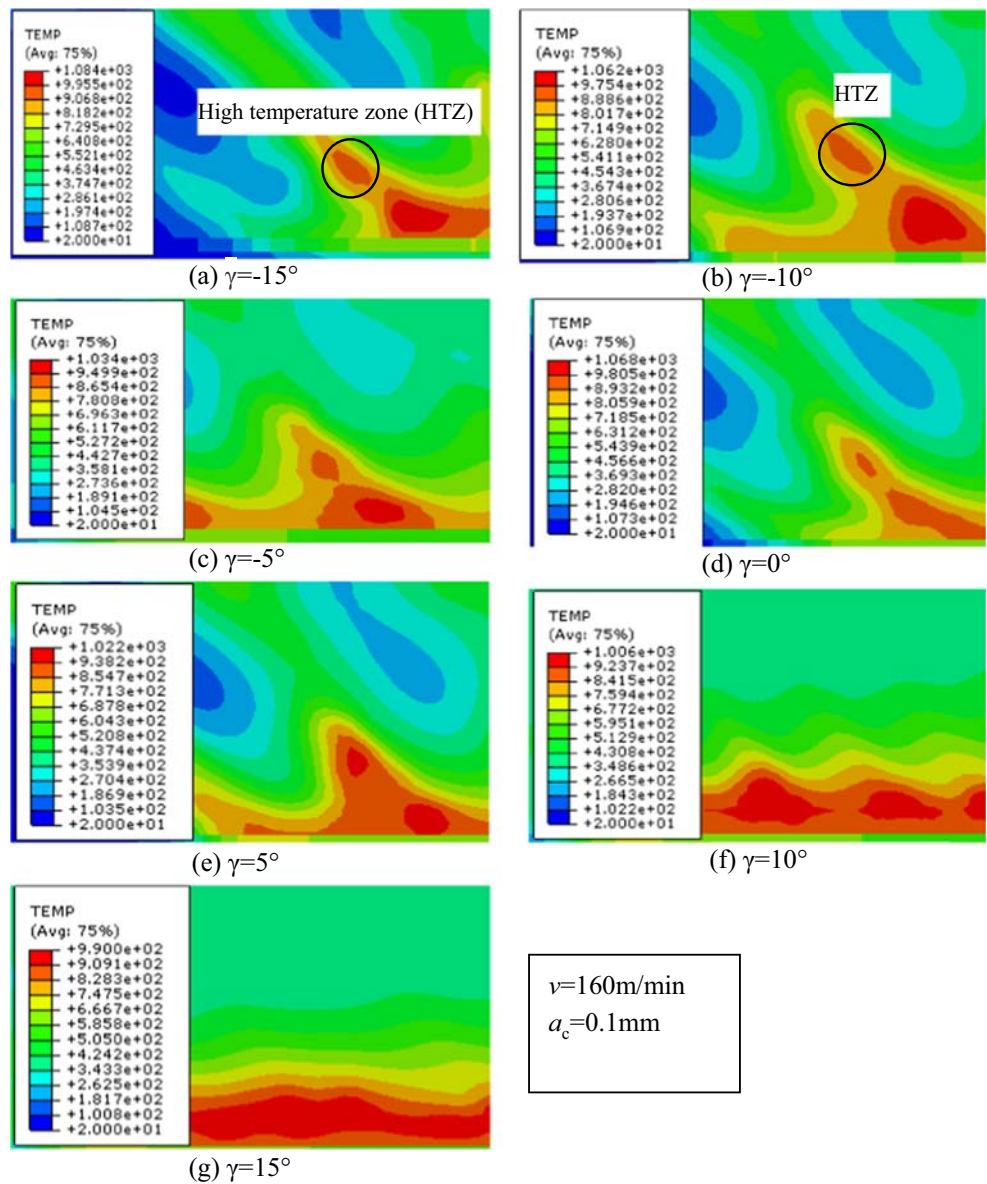
In the formation process of adiabatic shear, the shear zone material enters into the stage of toughness failure under the effect of the cutting tool. Figure 17 shows that the temperature and strain in adiabatic shear bands ( $\gamma = 0^\circ$ ,  $v = 100$  m/min,  $f = 0.1$  mm/rev) increase simultaneously at the same time, and the strain reaches the maximum value slightly later than temperature [34].

### 3.4 Formation mechanism analyses of serrated chips

From the cutting simulation results, it can be seen that the sawtooth of chips is more obvious when the cutting speed increases with the same tool rake angle. Figure 18 shows the temperature distribution of the undistorted nephogram of the shear band at different cutting speeds. The rake angle of the tool is  $0^\circ$  and the cutting thickness is 0.1 mm. It can be seen that the temperature of the shear band decreases gradually



**Fig. 20** High-temperature zone and tool-chip contact zone in an undeformed shape



along the direction of the shear plane. The local temperature in the shear zone increases due to the deformation heat caused by the uneven deformation of the material in the shear zone, which leads to the high-temperature zone.

The variation of temperature in HTZ with cutting speed is shown in Fig. 19. It can be seen that with the increase of cutting speed, the temperature in the high-temperature zone and the sawtooth degree of chips increase. When the cutting speed is 80 m/min, the temperature in the high-temperature zone is 790 °C, and with the increase of cutting speed to 200 m/min, the temperature in the high-temperature zone rises to 1048 °C. The reasons for this change are as follows: in the cutting process, with the increase of cutting speed, the cutting heat generated in the tool-chip contact zone increases, and the material softening degree in the shear zone is strengthened. Under the action of cutting tools, the material softening

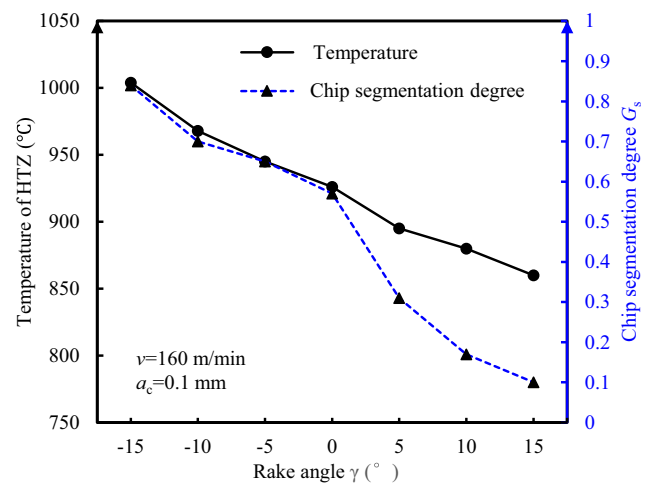


**Fig. 21** The variation of temperature and segmentation degree with different rake angle

increases the material deformation in the shear zone, which leads to an increase in deformation heat [35, 36]. Therefore, the temperature in the HTZ increases with the increase of cutting speed, the adiabatic shear degree of materials in the shear zone increases, and the sawtooth degree of chips also increases.

As shown in Fig. 20, using the results of the undeformed simulation, the temperature distribution of the adiabatic shear band during the chip formation process and high-temperature zone (HTZ) can be observed. The reasons of adiabatic shear formation are as follows: in the cutting process, the heat which is generated from the friction between the tool and material gathered at the tooltip, and the temperature rises in a short time. In the material surrounding the tooltip, the heat softening effect of the material is stronger than the strain hardening; with the movement of the cutting tool, the material of the shear zone is deformed. As the heat and deformation produce heat and material deformation promotes each other the shear zone instability, so there is serrated chip. The concentrated heat in the shear zone is mainly generated from the material conduction and deformation; the occurrence of HTZ is attributed and that the material deformation is non-uniform in the shear zone [37].

As shown in Fig. 21, it can be seen that the different rake angles lead to a degree of thermal softening effect and variation of temperature in HTZ. As a result, with the increase of the rake angle, the degree of adiabatic shear in the shear zone decreases and the chip segmentation degree increases. When the angle of the tool is  $-15^\circ$ , the temperature of the HTZ is  $1009^\circ\text{C}$ ; when the adiabatic shear zone is formed, the corresponding segmentation degree is 0.6. When the rake angle reaches  $15^\circ$ , the temperature in the HTZ is  $524^\circ\text{C}$  and the segmentation degree is 0.1.

## 4 Conclusion

1. The correctness of the finite element cutting simulation model is verified by the segmentation degree  $G_s$ . The variation of the rake angle and cutting parameters has a great influence on the chip morphology. The segmentation degree  $G_s$  increases with the increase of cutting speed and feed rate and decreases with the increase of rake angle. The segmentation degree has the largest reduction when the rake angle is in the range of  $0^\circ\sim 5^\circ$ , and it provides a theoretical basis for the selection of the rake angle during machining Ti-6Al-4V titanium alloy.
2. The stress value in the reference unit of the shear zone increases with the cutting tool closing, reaching a maximum of about 1600 MPa and then descending. The fluctuation range of the stress value is reduced when the rake angle of the tool increases. When the stress of the reference unit reaches the starting point of the damage, the material began to fail.
3. The results show that the occurrence of HTZ is the result of the combination of heat conduction and deformation heat in the formation of the shear zone. The temperature, the stress, and the strain change rapidly at the same time and form an adiabatic shear band in the cutting process. The temperature in the HTZ increases with the increase of cutting speed, the adiabatic shear degree of materials in the shear zone increases, and the sawtooth degree of chips also increases. With the increase of the rake angle, the degree of adiabatic shear in the shear zone decreases and chip segmentation degree increases.

**Funding information** The authors would like to acknowledge the financial support of the National Natural Science Foundation of China (51605260), the Key Research and Development Program of Shandong Province - Public Welfare Special (2017GGX30144, 2018GGX103043), and the Young Scholars Program of Shandong University (2018WLJH57).

## References

1. Ai X (2003) High speed machining technology. National Defense Industry Press, Beijing
2. Suo T, Wang C, Hang C (2016) Research status of adiabatic shear zone in dynamic deformation of materials. *Mech Sci Technol* 35(1): 1–9
3. Zener C, Hollomon JH (1946) Problems in non-elastic deformation of metals. *J Appl Phys* 17(2):69–82
4. Recht RF (1964) Catastrophic thermoplastic shear. *J Appl Mech* 31(2):189–193
5. Xiao D, Li Y, Cai L (2010) Progress in research on adiabatic shearing. *Exp Mech* 4:463–475
6. Tan C, Wang F, Li S (2003) Progresses and trends in researches on adiabatic shear deformation. *Ordnance Mater Sci Eng* 26(5):62–67
7. Xu Y, Bai Y (2007) Shear localization, microstructural evolution and fracture under high-strain rate. *Adv Mech* 37(4):496–516
8. Culver RS (1973) Thermal instability strain in dynamic plastic deformation. *Metallurgical effects at high strain rates*. Springer, Boston, p 519–530
9. Batra RC, Kim CH (1992) Analysis of shear banding in twelve materials. *Int J Plast* 8(4):425–452
10. Xu T, Wang L, Lu W (1987) The thermo-viscoplastic properties and adiabatic shear deformation for a titanium alloy Ti-6Al-4V under high strain rates. *Explos Shock Waves* 7(1):1–8
11. Hoffmeister HW, Gente A, Weber TH (1999) Chip formation at titanium alloys under cutting speed of up to 100m/s. In: 2nd Int Conf High Speed Mach, edited by Schulz H, Molinari A, Dudzinski D, PTW Darmstadt University 21–28
12. Turley DM, Doyle ED, Ramalingam S (1982) Calculation of shear strains in chip formation in titanium. *Mater Sci Eng* 55(1):45–48
13. Miguélez MH, Soldani X, Molinari A (2013) Analysis of adiabatic shear banding in orthogonal cutting of Ti alloy. *Int J Mech Sci* 75: 212–222
14. Zhang Y, Mabrouki T, Nelias D, Gong Y (2011) FE-model for titanium alloy (Ti-6Al-4V) cutting based on the identification of limiting shear stress at tool-chip interface. *Int J Mater Form* 4(1): 11–23
15. Zhang XP, Shivpuri R, Srivastava AK (2017) A new microstructure-sensitive flow stress model for the high-speed machining of titanium alloy Ti-6Al-4V. *J Manuf Sci Eng* 139(5): 051006

16. Li A, Pang J, Zhao J, Zang J, Wang F (2017) FEM-simulation of machining induced surface plastic deformation and microstructural texture evolution of Ti-6Al-4V alloy. *Int J Mech Sci* 123:214–223
17. Li A, Pang J, Zhao J (2019) Crystallographic texture evolution and tribological behavior of machined surface layer in orthogonal cutting of Ti-6Al-4V alloy. *J Mater Res Technol* 8(5):4598–4611
18. Zhou Y, Sun H, Li A, Lv M, Xue C, Zhao J (2019) FEM simulation-based cutting parameters optimization in machining aluminum-silicon piston alloy ZL109 with PCD tool. *J Mech Sci Technol* 33(7):3457–3465
19. Song X, Li A, Lv M, Lv H, Zhao J (2019) Finite element simulation study on pre-stress multi-step cutting of Ti-6Al-4V titanium alloy. *Int J Adv Manuf Technol* 104(5–8):2761–2771
20. Liu G, Shah S, Özel T (2019) Material ductile failure-based finite element simulations of chip serration in orthogonal cutting of titanium alloy Ti-6Al-4V. *J Manuf Sci Eng* 141(4):041017
21. Hou G, Li A, Song X, Sun H, Zhao J (2018) Effect of cutting parameters on surface quality in multi-step turning of Ti-6Al-4V titanium alloy. *Int J Adv Manuf Technol* 98(5–8):1355–1365
22. Davis B, Dabrow D, Ju L, Li A, Xu C, Huang Y (2017) Study of chip morphology and chip formation mechanism during machining of magnesium-based metal matrix composites. *J Manuf Sci Eng* 139(9):091008
23. Zang J, Zhao J, Li A, Pang J (2018) Serrated chip formation mechanism analysis for machining of titanium alloy Ti-6Al-4V based on thermal property. *Int J Adv Manuf Technol* 98(1–4):119–127
24. Li J, Xu B (2017) Study on adiabatic shearing sensitivity of titanium alloy in the process of different cutting speeds. *Int J Adv Manuf Technol* 93(5–8):1859–1865
25. Wang F, Zhao J, Li Z, Li A (2016) Coated carbide tool failure analysis in high-speed intermittent cutting process based on finite element method. *Int J Adv Manuf Technol* 83(5–8):805–813
26. Meng L (2013) Finite element modelling on high-speed milling process of titanium alloy. Shanghai Jiao Tong University, Master's Degree Thesis 13–16
27. Johnson GR, Cook WH (1983) A constitutive model and data for metals subjected to large strains, high strain rates and high temperature. *Proc 7th Int Sympo Ballistics, Netherlands* 541–547
28. Lee WS, Lin CF (1998) High-temperature deformation behavior of Ti6Al4V alloy evaluated by high strain-rate compression tests. *J Mater Process Technol* 75(1):127–136
29. Wang B, Liu Z (2015) Shear localization sensitivity analysis for Johnson–Cook constitutive parameters on serrated chips in high speed machining of Ti6Al4V. *Simul Model Pract Theory* 55:63–76
30. Johnson GR, Cook WH (1985) Fracture characteristics of three metals subjected to various strains, strain rates, temperatures and pressures. *Eng Fract Mech* 21(1):31–48
31. Davies MA, Chou Y, Evans CJ (1996) On chip morphology, tool wear and cutting mechanics in finish hard turning. *CIRP Ann Manuf Technol* 45(1):77–82
32. Wang F, Zhao J, Li A, Zhu N, Zhao JB (2014) Three-dimensional finite element modeling of high-speed end milling operations of Ti-6Al-4V. *Proc Inst Mech Eng Part B J Eng Manuf* 228(6):893–902
33. Li A, Zhao J, Hou G (2017) Effect of cutting speed on chip formation and wear mechanisms of coated carbide tools when ultra-high-speed face milling titanium alloy Ti-6Al-4V. *Adv Mech Eng* 9(7):1687814017713704
34. Chen G (2012) Cutting mechanism of aerospace light alloy based on ductile failure. *Tianjin University* 25–30
35. Ke Q, Xu D, Xiong D (2017) Cutting zone area and chip morphology in high-speed cutting of titanium alloy Ti-6Al-4V. *J Mech Sci Technol* 31(1):309–316
36. Li W, Xu D, Xiong D, Ke Q (2019) Compression deformation in the primary zone during the high-speed cutting of titanium alloy Ti-6Al-4V. *Int J Adv Manuf Technol* 102(9–12):4409–4417
37. Liu H, Zhang J, Xu X, Zhao W (2018) Experimental study on fracture mechanism transformation in chip segmentation of Ti-6Al-4V alloys during high-speed machining. *J Mater Process Technol* 257:132–140

**Publisher's note** Springer Nature remains neutral with regard to jurisdictional claims in published maps and institutional affiliations.